Zero-Offset Sections with a Deblurring Filter in the Time Domain

Shihang Feng[1], *Oz Yilmaz*[2,3], *Yuqing Chen*[1] *and Gerard T. Schuster*[1]
[1]*King Abdullah University of Science and Technology (KAUST)*
[2]*Anatolian Geophysical*
[3]*GeoTomo LLC*

SUMMARY

We present a workflow for reconstructing a high-quality zero-offset reflection section from prestack data. This workflow constructs a migration image volume by prestack time migration (PSTM) using a series of constant-velocity models. A deblurring filter for each constant-velocity model is applied to each time-migration image to get a deblurred image volume. In order to preserve all events in the image volume, each deblurred image panel is demigrated and then summed over the velocity axis. The resulting demigration section is equivalent to a zero-offset reflection section. Compared with the workflow without a deblurring filter, the composite zero-offset reflection section has higher resolution and a better signal-to-noise ratio. Numerical tests are used to validate the effectiveness of this method with both synthetic and field data.

INTRODUCTION

Seismic imaging problems can be separated into two parts: focusing and positioning (Kim et al., 1997). These two problems can be solved step by step. The zero-offset section can be obtained by a series of constant-velocity PSTM followed by time-migration velocity analysis and poststack demigration. Then poststack depth migration is applied for proper positioning of reflectors (Deregowski, 1990; Bloor and Deregowski, 2005; Zhang et al., 2002; Lee et al., 2008). This method has several advantages: 1) it allows for zero-offset extrapolation of the seismic data obtained for non-zero offsets, even in the case of complicated kinematics (Lailly et al., 1998), 2) PSTM is less sensitive to velocity errors and velocity information can be obtained using time-migration velocity analysis (Kim et al., 1997), 3) the cost of poststack migration is less than prestack depth migration for updating the velocity model.

A workflow is designed to get velocity independent zero-offset gathers and therefore circumvent the velocity uncertainty problem instead of eliminating the velocity uncertainties (Yilmaz, 2017, 2018). Instead of building a velocity model using time-migration velocity analysis, all the time-migration images are demigrated and summed to obtain a composite zero-offset section.

One of the problems with the above workflow is that the migration image can be polluted with artifacts associated with a poor source-receiver geometry and a limited migration aperture. This can significantly affect the quality of the interpretation as well as the estimation of the velocity model. In this paper we propose to mitigate these two problems by the application of migration deconvolution (Hu and Schuster, 1998; Yu et al., 2006; Aoki and Schuster, 2009) to the time migrated image.

This paper is divided into four sections. After the introduction, the second section presents the theory that combines a deblurring filter with PSTM to obtain the zero-offset section. The third section presents numerical tests of our MD time-migration strategy on synthetic and field data. The conclusions are given in the last section.

THEORY

Construction of the Zero-offset Wavefield

For a constant-velocity model, the sequence of NMO, DMO, CMP stack, and poststack migration operations are kinematically equivalent to prestack migration (Judson et al., 1978; Yilmaz and Claerbout, 1980; Hale, 1984). Following Yilmaz (2001, 2017), this statement can be expressed by the following equation:

$$\mathbf{L}^T_{post}\mathbf{d}_{post} = \mathbf{L}^T_{pre}\mathbf{d}_{pre}, \tag{1}$$

where $\mathbf{L}^T_{post}$ stands for poststack time-migration operator and $\mathbf{L}^T_{pre}$ represents the PSTM operater. Here, $\mathbf{d}_{post}$ is the zero-offset section obtained by the application of NMO, DMO and CMP stack and $\mathbf{d}_{pre}$ is the prestack data before processing. Yilmaz (2017) utilized this equivalence to construct the zero-offset wavefield. Demigration is treated as the inversion of poststack time migration $(\mathbf{L}^T_{post})^{-1}$ and applied to both sides of equation 1 to get:

$$\mathbf{d}_{post} = (\mathbf{L}^T_{post})^{-1}\mathbf{L}^T_{pre}\mathbf{d}_{pre}. \tag{2}$$

This implies that the zero-offset wavefield can be obtained by PSTM followed by demigration.

Alternatively, in this paper, we represent the demigration operator as $\mathbf{L}_{post}$. Then we modify equation 1, by adding the deblurring operator $\mathbf{F}_{post}$ to both sides of this equation to get:

$$\mathbf{F}_{post}\mathbf{L}^T_{post}\mathbf{d}_{post} = \mathbf{F}_{post}\mathbf{L}^T_{pre}\mathbf{d}_{pre}. \tag{3}$$

Then the demigration operator $\mathbf{L}_{post}$ is applied to both sides to get

$$\mathbf{L}_{post}\mathbf{F}_{post}\mathbf{L}^T_{post}\mathbf{d}_{post} = \mathbf{L}_{post}\mathbf{F}_{post}\mathbf{L}^T_{pre}\mathbf{d}_{pre}. \tag{4}$$

The matching filter $\mathbf{F}_{post} \approx (\mathbf{L}^T_{post}\mathbf{L}_{post})^{-1}$ can be calculated from the reference images and reference migration images, then

$$\mathbf{L}_{post}\mathbf{F}_{post}\mathbf{L}^T_{post} \approx \mathbf{L}_{post}(\mathbf{L}^T_{post}\mathbf{L}_{post})^{-1}\mathbf{L}^T_{post} = \mathbf{I}, \tag{5}$$

we have

$$\mathbf{d}_{post} = \mathbf{L}_{post}\mathbf{F}_{post}\mathbf{L}^T_{pre}\mathbf{d}_{pre}. \tag{6}$$

10.1190/segam2018-2996099.1

Equation 6 says that the zero-offset reflection section can be constructed by the demigration of the deblurred PSTM images. This formulation differs from that of Yilmaz (2017, 2018) in that deblurring filter is incorporated to suppress the migration artifacts in PSTM.

Workflow

Following Yilmaz (2017, 2018), the workflow for constructing a zero-offset reflection section is presented in Figure 1, where the goal is to get a zero-offset reflection section without committing to a velocity model.

(1) Perform PSTM on all the shot gathers using a series of constant-velocity models as in Figure 1b. The set of images form an image volume in (V,X,T) coordinates, where V is the rms velocity, X is the midpoint, and T is the event time.

(2) Build a reference grid model in (V,X,T) coordinates. Simulate the reference data using Born modeling with the same constant-velocity model used for PSTM in step 1.

(3) Apply PSTM to the reference data using the same series of constant-velocity models. The set of migration image panels form a reference migration volume in the (V,X,T) coordinates as shown in Figure 1c.

(4) Use the reference migration volume and the reference model to calculate the deblurring filter for each constant-velocity model. Then apply these deblurring filters to each migration image to get a series of deblurred migration panels and the deblurred migration cube as shown in Figure 1d.

(5) Demigrate each of the deblurred migration panels employing the same constant-velocity model used for PSTM in step 1 to create a zero-offset volume in the (V,X,T) coordinates as in Figure 1f.

(6) Apply a Radon transform to each of the velocity gathers in the (V,T) panels to reduce the horizontal smearing of amplitudes.

(7) Sum over the velocity axis to obtain a composite zero-offset reflection section that preserves all of the reflections and diffractions as shown in Figure 1e.

Bandpass and Cadzow filters can be applied in the workflow to increase the signal-to-noise ratio of the composite zero-offset section. Time-migration velocity analysis can be applied in step (1) or step (4) to give a velocity model for poststack migration of the zero-offset section. The details are shown in Appendix A.

NUMERICAL EXAMPLES

This workflow is now applied to synthetic data generated from a point-scatterer model and the overthrust model. In addition, we apply this method to field data recorded in the Gulf of Mexico.

Overthrust Model

The overthrust model is shown in Figure 2, where the model size is 4 km in the X direction and 1.6 km in the Z direction with a grid spacing of 10 m. One hundred sources are located on the surface with a spacing of 40 m, and the traces are recorded by 400 receivers spaced with an interval of 10 m on the surface. The source wavelet is a Ricker wavelet with a peak frequency of 15 Hz.

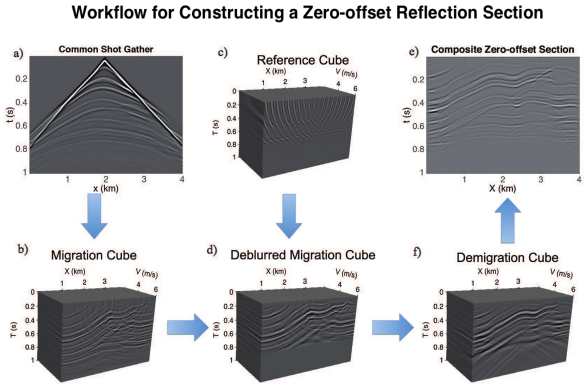

Figure 1: The workflow for constructing a zero-offset reflection section.

Figure 3 compares the true and composite zero-offset sections before and after deblurring. The deblurred zero-offset reflection section has fewer artifacts and greater similarity with the true zero-offset section than the section without filtering, especially in the red box. Figure 4 shows the frequency spectrum of the zero-offset sections. The yellow line represents the spectrum of the zero-offset section with deblurring. It clearly shows an improvement in resolution when compared with the zero-offset section without deblurring indicated by the red line and it is similar to the true zero-offset section indicated by the blue line.

GOM Data

The proposed method is now tested on a 2D marine data set. There are 100 shots with a shot interval of 37.5 m, and each shot is recorded by a 6 km long cable with 480 receivers spaced with a 12.5 m receiver interval. The shortest offset is 200 m and the data is filtered by a 25-Hz Wiener filter (Boonyasiriwat et al., 2009). Here the source wavelet is extracted from the raw data by stacking the time-shifted reflection events together from 200 to 250 m offset in the shot gather. The reflection traveltimes are then used to shift the traces so the reflection events from the same interface are flattened. These flattened reflection events are stacked together to get an estimate of the source wavelet.

There is no true zero-offset section for this data since the minimum offset is 200 m. Thus the common offset gather (COG) shown in Figure 5a at $x = 200$ m is regarded as an approximation of the zero-offset section. Compared with the COG at 200 m, the composite zero-offset sections with and without deblurring in Figure 5b and 5c contains all the reflections and diffractions in the pseudo zero-offset section. The zoom views of these zero-offset sections are compared in Figure 6, in which the red arrows point to the areas with noticeable improvements in resolution.

10.1190/segam2018-2996099.1

Time-migration velocity analysis can be applied to build a series of semblance spectrua as shown in Figure 8a. To build a velocity model, we use automatic velocity picking with the algorithm described by Fomel (2009). Figure 8b shows a result of the 2D RMS velocity picked from the semblance panels. To transform this velocity model into the depth domain, we use the Dix conversion formula (Dix, 1955) to construct the interval velocity model shown in Figure 8c. Due to undesirable velocity errors generated by errors in the semblance picking and Dix conversion, some of the reflection events in the prestack image will be mispositioned, defocused and even missing. The Kirchhoff prestack migration image and its zoom view are shown in Figures 9a, 10a and 10d, respectively. In the areas denoted by red arrows, we can clearly see that the events are missing. Now, the composite zero-offset section without and with deblurring are migrated by Kirchhoff poststack migration, where the images and their zoom views are shown in Figures 9b, 9c , 10b, 10c, 10e and 10f. respectively. All the events are preserved in the poststack migration images. Moreover, the poststack migration image with the composited deblurred zero-offset section shows improved amplitude balance and resolution of the image when compared to the image without deblurring. The increase in spatial resolution is further validated by the vertical-wavenumber spectra in Figure 11.

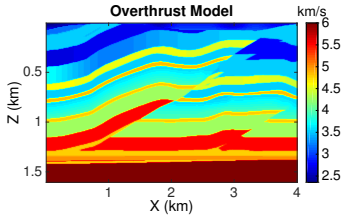

Figure 2: The overthrust model.

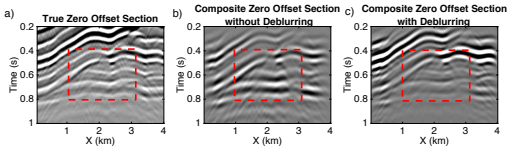

Figure 3: a) The true zero-offset reflection sections, the composite zero-offset section b) without and c) with deblurring using overthrust data.

CONCLUSIONS

We present a time-domain MD workflow that combines the deblurring filter with the workflow proposed by Yilmaz (2017, 2018) to improve the quality of zero-offset reflection sections. The deblurring filters are calculated from a reference model with evenly distributed point scatterers in the (X,T) domain and its corresponding time-migration images. Numerical tests on synthetic and field data show the proposed workflow can significantly improve the resolution of the zero-offset reflection section and suppress the migration artifacts compared to the workflow without deblurring. The limitation of this procedure is that the deblurring filter can increase the noise level as well as the image resolution of the final zero-offset reflection unless the data are properly denoised and the filter has sufficient regularization. Thus the removal of noise from data is important for the application of the deblurring filter.

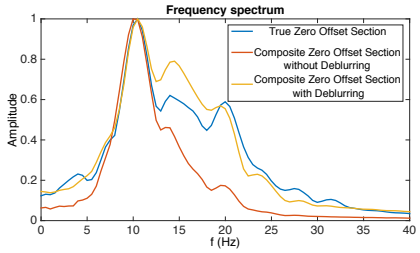

Figure 4: The frequency spectrum of the true zero-offset reflection sections, the composite zero-offset section without and with deblurring using overthrust data.

ACKNOWLEDGEMENTS

The research reported in this publication was supported by the King Abdullah University of Science and Technology (KAUST) in Thuwal, Saudi Arabia. We are grateful to the sponsors of the Center for Subsurface Imaging and Modeling Consortium for their financial support. For computer time, this research used the resources of the Supercomputing Laboratory at KAUST and the IT Research Computing Group. We thank them for providing the computational resources required for carrying out this work.

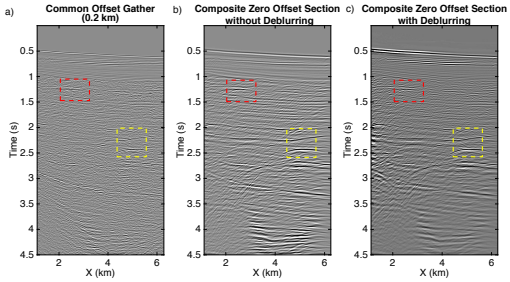

Figure 5: a) The common offset gather at 200 m, the composite zero-offset section b) without and c) with deblurring for the GOM data.

10.1190/segam2018-2996099.1

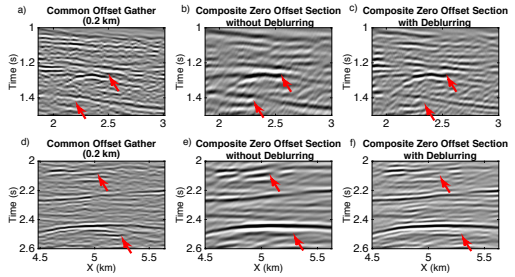

Figure 6: Top row: zoom views of the red box in the gathers from a) the common offset gather at 200 m, the composite zero-offset section b) without and c) with deblurring for the GOM data. Bottom row: zoom views of the yellow box in the gathers from d) the common offset gather at 200 m, the composite zero-offset section e) without and f) with deblurring for the GOM data

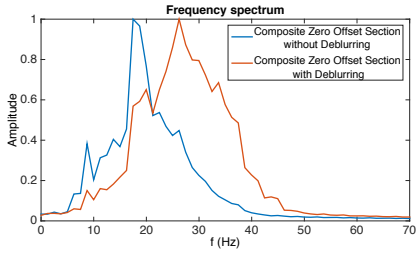

Figure 7: The frequency spectrum of the composite zero-offset section without and with deblurring for the GOM data.

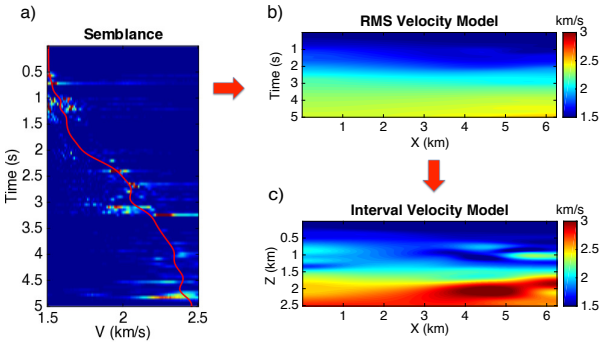

Figure 8: a) The semblance spectrum of the GOM data using time-migration velocity analysis (red line indicates the RMS velocity picks). b) The RMS velocity model obtained from velocity picking. c) The interval velocity model obtained from the Dix conversion.

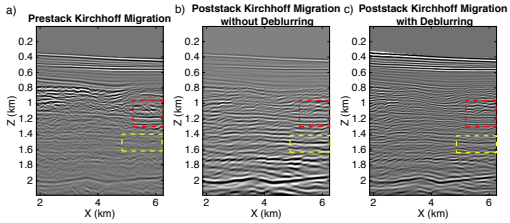

Figure 9: The images from a) the prestack Kirchhoff migration, the poststack Kirchhoff migration using the composite zero-offset section b) without and c) with deblurring using the GOM data.

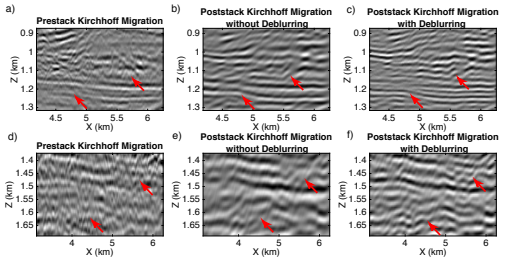

Figure 10: Top row: zoom views of the red box in the images from a) prestack Kirchhoff migration, poststack Kirchhoff migration using composite zero-offset section b) without and c) with deblurring using the GOM data. Bottom row: zoom views of the yellow box in the images from d) prestack Kirchhoff migration, poststack Kirchhoff migration using the composite zero-offset section e) without and f) with deblurring using the GOM data.

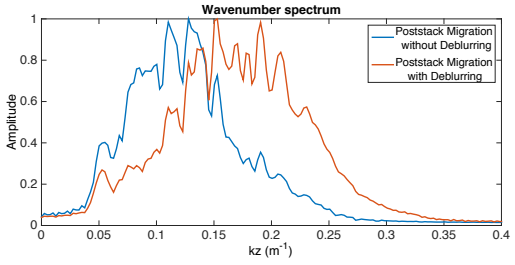

Figure 11: The wavenumber spectrum of the images from a) prestack Kirchhoff migration, poststack Kirchhoff migration using the composite zero-offset section b) without and c) with deblurring using the GOM data.

10.1190/segam2018-2996099.1

REFERENCES

Aoki, N., and G. T. Schuster, 2009, Fast least-squares migration with a deblurring filter: Geophysics, **74**, WCA83–WCA93.

Bloor, R. I., and S. M. Deregowski, 2005, Demigration to zero offset: SEG Technical Program Expanded Abstracts 1995, 1433–1436.

Boonyasiriwat, C., P. Valasek, P. Routh, W. Cao, G. T. Schuster, and B. Macy, 2009, An efficient multiscale method for time-domain waveform tomography: Geophysics, **74**, WCC59–WCC68.

Caers, J., 2011, Modeling Uncertainty in the Earth Sciences: John Wiley & Sons.

Chen, Y., G. Dutta, W. Dai, and G. T. Schuster, 2017, Q-least-squares reverse time migration with viscoacoustic deblurring filters: Geophysics, **82**, S425–S438.

Dai, W., J. Schuster, et al., 2009, Least-squares migration of simultaneous sources data with a deblurring filter: SEG Technical Program Expanded Abstracts 2009, 2990–2994.

Dai, W., X. Wang, and G. T. Schuster, 2011, Least-squares migration of multisource data with a deblurring filter: Geophysics, **76**, R135–R146.

Deregowski, S., 1990, Common-offset migrations and velocity analysis: First Break, **8**, 225–234.

Dix, C. H., 1955, Seismic velocities from surface measurements: Geophysics, **20**, 68–86.

Fomel, S., 2009, Velocity analysis using AB semblance: Geophysical Prospecting, **57**, 311–321.

Fomel, S., and E. Landa, 2014, Structural uncertainty of time-migrated seismic images: Journal of Applied Geophysics, **101**, 27–30.

Glogovsky, V., E. Landa, S. Langman, and T. J. Moser, 2009, Validating the velocity model: The Hamburg score: First Break, **27**.

Grubb, H., A. Tura, and C. Hanitzsch, 2001, Estimating and interpreting velocity uncertainty in migrated images and AVO attributes: Geophysics, **66**, 1208–1216.

Hale, D., 1984, Dip-moveout by Fourier transform: Geophysics, **49**, 741–757.

Hu, J., and G. T. Schuster, 1998, Migration deconvolution: SPIE's International Symposium on Optical Science, Engineering, and Instrumentation, International Society for Optics and Photonics, 118–124.

Hu, J., G. T. Schuster, and P. A. Valasek, 2001, Poststack migration deconvolution: Geophysics, **66**, 939–952.

Judson, D., P. Schultz, and J. Sherwood, 1978, Equalizing the stacking velocities of dipping events via devilish: Geophysical Prospecting, 669–669.

Kim, Y. C., W. B. Hurt Jr, L. J. Maher, and P. J. Starich, 1997, Hybrid migration: A cost-effective 3-D depth-imaging technique: Geophysics, **62**, 568–576.

Lailly, P., B. Duquet, and A. Ehinger, 1998, Processing method for obtaining zero-offset seismic data by depth domain stacking. (US Patent 5,808,964).

Lee, S.-S., J. Willis, and Y. Lin, 2008, Method for depth migrating seismic data using pre-stack time migration, demigration, and post-stack depth migration. (US Patent 7,388,808).

Schuster, G., G. Zhan, W. Dai, and C. Boonyasiriwat, 2010, Acoustic multi-source waveform inversion with deblurring: Presented at the 72nd EAGE Conference and Exhibition incorporating SPE EUROPEC 2010.

Schuster, G. T., and J. Hu, 2000, Green's function for migration: Continuous recording geometry: Geophysics, **65**, 167–175.

Yilmaz, Ö., 2001, Seismic data analysis: Processing, inversion, and interpretation of seismic data: Society of Exploration Geophysicists.

———, 2017, Circumventing velocity uncertainty in imaging complex structures: SEG Technical Program Expanded Abstracts 2017, 5706–5710.

———, 2018, Circumventing velocity uncertainty in imaging complex structures: The Leading Edge, **37**, 14–18.

Yilmaz, Ö. g. . a., and J. F. Claerbout, 1980, Prestack partial migration: Geophysics, **45**, 1753–1779.

Yu, J., J. Hu, G. T. Schuster, and R. Estill, 2006, Prestack migration deconvolution: Geophysics, **71**, S53–S62.

Zhang, Y., M. Karazincir, C. Notfors, J. Sun, and B. Hung, 2002, Amplitude preserving v(z) prestack Kirchhoff migration, demigration and modeling: migration, **8**, 3.

10.1190/segam2018-2996099.1

REFERENCES

Aoki, N., and G. T. Schuster, 2009, Fast least-squares migration with a deblurring filter: Geophysics, **74**, no. 6, WCA83–WCA93, https://doi.org/10.1190/1.3155162.

Bloor, R. I., and S. M. Deregowski, 2005, Demigration to zero offset: 75th Annual International Meeting, SEG, Expanded Abstracts, 1433–1436, https://doi.org/10.1190/1.1887230.

Boonyasiriwat, C., P. Valasek, P. Routh, W. Cao, G. T. Schuster, and B. Macy, 2009, An efficient multiscale method for time-domain waveform tomography: Geophysics, **74**, no. 6, WCC59–WCC68, https://doi.org/10.1190/1.3151869.

Caers, J., 2011, Modeling uncertainty in the earth sciences: John Wiley & Sons.

Chen, Y., G. Dutta, W. Dai, and G. T. Schuster, 2017, Q-leastsquares reverse time migration with viscoacoustic deblurring filters: Geophysics, **82**, no. 6, S425–S438, https://doi.org/10.1190/geo2016-0585.1.

Dai, W., and J. Schuster, 2009, Least-squares migration of simultaneous sources data with a deblurring filter: 79th Annual International Meeting, SEG, Expanded Abstracts, 2990–2994, https://doi.org/10.1190/1.3255474.

Dai, W., X. Wang, and G. T. Schuster, 2011, Least-squares migration of multisource data with a deblurring filter: Geophysics, **76**, no. 5, R135–R146, https://doi.org/10.1190/geo2010-0159.1.

Deregowski, S., 1990, Common-offset migrations and velocity analysis: First Break, **8**, 225–234, https://doi.org/10.3997/1365-2397.1990011.

Dix, C. H., 1955, Seismic velocities from surface measurements: Geophysics, **20**, 68–86, https://doi.org/10.1190/1.1438126.

Fomel, S., 2009, Velocity analysis using AB semblance: Geophysical Prospecting, **57**, 311–321, https://doi.org/10.1111/j.1365-2478.2008.00741.x.

Fomel, S., and E. Landa, 2014, Structural uncertainty of timemigrated seismic images: Journal of Applied Geophysics, **101**, 27–30, https://doi.org/10.1016/j.jappgeo.2013.11.010.

Glogovsky, V., E. Landa, S. Langman, and T. J. Moser, 2009, Validating the velocity model: The Hamburg score: First Break, **27**.

Grubb, H., A. Tura, and C. Hanitzsch, 2001, Estimating and interpreting velocity uncertainty in migrated images and AVO attributes: Geophysics, **66**, 1208–1216, https://doi.org/10.1190/1.1487067.

Hale, D., 1984, Dip-moveout by Fourier transform: Geophysics, **49**, 741–757, https://doi.org/10.1190/1.1441702.

Hu, J., and G. T. Schuster, 1998, Migration deconvolution: SPIE's International Symposium on Optical Science, Engineering, and Instrumentation, International Society for Optics and Photonics, 118–124.

Hu, J., G. T. Schuster, and P. A. Valasek, 2001, Poststack migration deconvolution: Geophysics, **66**, 939–952, https://doi.org/10.1190/1.1444984.

Judson, D., P. Schultz, and J. Sherwood, 1978, Equalizing the stacking velocities of dipping events via devilish: Geophysical Prospecting, 669–669.

Kim, Y. C., W. B. Hurt Jr, L. J. Maher, and P. J. Starich, 1997, Hybrid migration: A cost-effective 3-D depth-imaging technique: Geophysics, **62**, 568–576, https://doi.org/10.1190/1.1444166.

Lailly, P., B. Duquet, and A. Ehinger, 1998, Processing method for obtaining zero-offset seismic data by depth domain stacking: U.S. Patent 5,808,964.

Lee, S.-S., J. Willis, and Y. Lin, 2008, Method for depth migrating seismic data using pre-stack time migration, demigration, and post-stack depth migration: U.S. Patent 7,388,808.

Schuster, G. T., and J. Hu, 2000, Green's function for migration: Continuous recording geometry: Geophysics, **65**, 167–175, https://doi.org/10.1190/1.1444707.

Schuster, G. T., G. Zhan, W. Dai, and C. Boonyasiriwat, 2010, Acoustic multi-source waveform inversion with deblurring: Presented at the 72nd Annual International Conference and Exhibition, EAGE, Extended Abstracts, https://doi.org/10.3997/2214-4609.201400800.

Yilmaz, O., 2001, Seismic data analysis: Processing, inversion, and interpretation of seismic data: SEG.

Yilmaz, O., 2017, Circumventing velocity uncertainty in imaging complex structures: 87th Annual International Meeting, SEG, Expanded Abstracts, 5706–5710, https://doi.org/10.1190/segam2017-17415496.1.

Yilmaz, O., 2018, Circumventing velocity uncertainty in imaging complex structures: The Leading Edge, **37**, 14–18, https://doi.org/10.1190/tle37010014.1.

Yilmaz, O. A., and J. F. Claerbout, 1980, Prestack partial migration: Geophysics, **45**, 1753–1779, https://doi.org/10.1190/1.1441064.

Yu, J., J. Hu, G. T. Schuster, and R. Estill, 2006, Prestack migration deconvolution: Geophysics, **71**, no. 2, S53–S62, https://doi.org/10.1190/1.2187783.

Zhang, Y., M. Karazincir, C. Notfors, J. Sun, and B. Hung, 2002, Amplitude preserving v(z) prestack Kirchhoff migration, demigration and modeling: Migration, **8**.